

Correlated X-ray and Optical Variability in Mkn 509

Kevin Marshall^{1,2}, Wesley T. Ryle², H. Richard Miller²

ABSTRACT

We present results of a 3 year monitoring campaign of the Seyfert 1 galaxy Markarian 509, using X-ray data from the *Rossi X-ray Timing Explorer* and optical data taken by the SMARTS consortium. Both light curves show significant variations, and are strongly correlated with the optical flux leading the X-ray flux by 15 days. The X-ray power spectrum shows a steep high-frequency slope of -2.0 , breaking to a slope of -1.0 at a timescale of 34 days. The lag from optical to X-ray emission is most likely caused by variations in the accretion disk propagating inward.

Subject headings: galaxies: active — galaxies: Seyfert — galaxies: individual (Mkn 509)

1. Introduction

Variability has long been recognized as one of the defining characteristics of active galactic nuclei (AGN). This variability is not limited to one wavelength regime, but is spread across the entire electromagnetic spectrum. Produced in the innermost regions of the nucleus are X-ray and optical/UV continuum photons. Current models involve an accretion disk emitting thermal (10^5 K) photons in the optical and UV range (Malkan 1983; Shields 1978), which are then inverse Compton scattered to X-ray energies by a corona of hot electrons above the accretion disk (Haardt & Maraschi 1991, 1993).

By monitoring the variability at optical and X-ray wavelengths, we can learn information about the geometry and exact mechanism responsible for the emission. The traditional view is that because the X-rays are produced closer to the nucleus, variations should be the largest at that wavelength, with optical variations lagging behind. On the other hand, the variations may originate in the optical seed photons, which then cause the X-ray emission to lag behind the optical.

¹Department of Physics, Bucknell University, Lewisburg PA 17837, kevin.marshall@bucknell.edu

²Department of Physics and Astronomy, Georgia State University, Atlanta, GA 30303

Previous attempts at correlating X-ray and optical variability in Seyfert galaxies have been inconclusive. On long timescales, Uttley et al. (2003) detected a strong correlation in NGC 5548 with no lag, while Chiang et al. (2000) found a weaker correlation on short timescales. The same was true for NGC 4051, with Peterson et al. (2000) finding a correlation on long but not short timescales. However this is not the case with all Seyferts, as Maoz et al. (2002) found no correlation in NGC 3516 after 5 years of monitoring. Shemmer et al. (2003) and Arévalo et al. (2005) both found correlations on short timescales in NGC 4051 and MCG–6-30-15, respectively, while Papadakis et al. (2000) found no correlation on short timescales in Akn 564. For a more comprehensive review of past efforts, see Maoz et al. (2002) and references therein.

Mkn 509 is a nearby ($z = 0.034$) Seyfert 1 galaxy. First detected in the X-rays by *Ariel V* (Cooke et al. 1978), Mkn 509 was later found to have a soft X-ray excess by Singh et al. (1989). Simultaneous observations with *GINGA* and *ROSAT* again showed a soft excess, with some flattening at higher energies due to reflection (Pounds et al. 1994). Later observations with *ASCA* showed the presence of an Fe $K\alpha$ line at 6.4 keV, and the presence of a warm absorber rather than a soft excess (Reynolds 1997). More recent observations with *XMM-Newton* show the origin of the soft X-ray excess lies mostly in thermal emission from the inner parts of the accretion disk (Pounds et al. 2001).

We present here results from a 3.5 year X-ray and optical monitoring campaign on Mkn 509. In §2, we show light curves and discuss data analysis methods for all of our observations. In §3, we calculate the X-ray power density spectrum (PDS), using Monte Carlo methods. In §4, we present results of cross-correlation between the X-ray and optical light curves and discuss the significance of the results. Finally, in §5 we compare our result to previous efforts, and discuss possible implications for physical models of accretion.

2. Observations and Data Reduction

2.1. X-ray Data

Mkn 509 was observed with the *Rossi X-ray Timing Explorer (RXTE)* from 28 March 2003 – 29 June 2006 in X-rays, with sampling every 3 days. We use only data taken by PCUs 0 and 2, in STANDARD2 data mode. All of our data were reduced using FTOOLS v5.2 software, provided by HEASARC. Data were excluded if the Earth elevation angle was $< 15^\circ$, pointing offset $> 0.02^\circ$, time since South Atlantic Anomaly passage < 30 minutes, or electron noise > 0.01 units. Counts were extracted from the top PCU layer only to maximize the signal to noise ratio.

2.2. Optical Data

Ground-based optical observations were taken roughly twice per week from 23 October 2003 – 12 November 2006, as weather conditions and proximity to the sun allowed. All data were taken with the 1.3m telescope at Cerro Tololo Inter-American Observatory (CTIO), operated by the SMARTS consortium. The 1.3m reflector uses the ANDICAM instrument, which has a Fairchild 447 2048 × 2048 CCD chip with 15 μm pixels. Using 2 × 2 binning, this yields a 6-arcminute field of view, with a plate scale of 0.369'' per pixel. Observations were taken in standard Johnson *BVR* filters; however we present only the *R* filter data here.

Image processing was done with IRAF, using standard methods. A large number (typically 10) of bias and flat fields were taken each night, and then combined using a min/max rejection algorithm in IRAF.

Photometry was done using the CCDPHOT program, developed for IDL by Marc Buie. A 7'' aperture was chosen to minimize any contributions from the host galaxy. Photometric measurements were taken for the object and check stars A and F from Miller (1981). We use differential photometry, i.e. no standard stars were used. Object brightness was calculated by comparison with check star A, and error bars are given by the standard deviation of the difference in brightness between check stars A and F.

3. Light Curves and the Power Density Spectrum

The X-ray and optical light curves are shown in Figure 1, and optical magnitudes are given in Table 1. The X-ray data are more complete, owing to weather and other observing constraints with ground-based telescopes. The X-ray data also show more high-frequency variability than the optical data.

To begin to quantify the intrinsic variability of each light curve, we have calculated the fractional variability, defined as

$$F_{\text{var}} = \sqrt{\frac{S^2 - \langle \sigma_{\text{err}}^2 \rangle}{\langle \mu \rangle^2}}$$

where S^2 is the variance of the light curve, $\langle \sigma_{\text{err}}^2 \rangle$ is the mean error squared, and $\langle \mu \rangle$ is the mean count rate (Markowitz & Edelson 2004). For Mkn 509, we find a fractional variability of $F_{\text{var}} = 19\%$ and 12% for the X-ray and optical light curves, respectively. Note

that we do not subtract any host galaxy flux from the optical data, so this figure represents a lower limit on the true value of F_{var} .

We use the Monte Carlo method of Uttley et al. (2002) and Markowitz et al. (2003) to calculate the power density spectrum (PDS). Briefly, a long light curve is simulated using the method of Timmer & Koenig (1995). This light curve is then split into parts, and the PDS calculated for each segment. The individual power spectra are then averaged, and then compared to the observed power spectrum. This is done over a grid of slopes and break frequencies.

For Mkn 509, we fixed the low frequency slope of the PDS at -1.0 , breaking to a steeper slope at some break frequency, ν_b . We use high-frequency slopes between -1.0 and -2.5 for our input models, and break frequencies between $-8.0 \leq \nu_b \leq -5.5$ Hz, incrementing the slope by 0.1 and the break frequency by factors of 1.5 (0.18 in the logarithm).

The simulation results are shown in Figure 2. The best fit occurs at a high frequency slope of -2.0 and a break frequency of $\nu_b = -6.47$ Hz, or a timescale of 34 days. The probability of acceptance of this 95%. For an unbroken power law, the probability of acceptance was only 29%, with a single slope of -1.2 .

Note that the PDS covers only slightly more than 2 decades in frequency, due to the lack of additional high-frequency data. We have proposed for more intensive observations with *RXTE*, which will allow us to fill in the high-frequency area of the PDS. Until then, the break timescale of 34 days should be regarded more as an upper limit and not a concrete value.

A break timescale less than 34 days does agree well with the mass-break frequency relationship discussed by Uttley & McHardy (2005) and Markowitz et al. (2003). With a black hole mass of $1.43 \times 10^8 M_\odot$ (Peterson et al. 2004), we would expect to find a break timescale of $\tau \sim 10 - 50$ days. Again, more high-frequency observations are needed to better constrain this value.

4. Cross Correlation Function

To examine the possibility of a correlation between X-ray and optical flux, we use the cross correlation function (CCF). The traditional CCF requires evenly sampled data, and can be computationally intensive. Because of observing constraints, neither our X-ray nor optical data are evenly sampled. To solve this issue, we use the discrete correlation function (DCF) of Edelson & Krolik (1988), which allows for cross-correlation of two unevenly sampled data

sets.

The DCF is shown in Figure 3, with the convention that positive lag indicating optical variations leading the X-rays. The maximum value occurs at a lag of $\tau = +15$ days, with a correlation coefficient of $r = 0.93$.

As discussed in Uttley et al. (2003), traditional error bars are inadequate for assessing the significance of the DCF, because adjacent data points in the light curve are “red noise” data and not uncorrelated. Therefore, similar to Uttley et al. (2003), we use Monte Carlo simulations to test the significance of both the correlation and measured lag in our DCF.

We began by simulating 2 independent red noise light curves, using the method of Timmer & Koenig (1995). Both light curves were given underlying model power spectra with slope -1 at low frequencies, breaking to a slope of -2 above a break frequency of $\log \nu = -6.47$. The two light curves were then re-sampled in the same fashion as the original data, and random noise was added in the form of a Gaussian random with mean of zero and standard deviation equal to the average observed error. For 10^4 simulations, we found a maximum correlation coefficient $r > 0.93$ only 38 times. Therefore the correlation coefficient of $r = 0.93$ seen in the data is significant at more than 99% confidence.

To test the significance of the measured lag, we use simulations similar to above. In this case, 2 identical light curves were generated, with one lagging 15 days behind the other. The simulated data were then re-sampled in the same fashion as the observed light curves, and random noise was added using the same method as above. We then searched for cases where the peak lag was greater than the lag at 15 days. Out of 10^4 simulations, we found only 287 cases where the peak lag did not occur at $\tau = 15$ days. Therefore our measured lag is significant at more than 97% confidence.

5. Conclusions

We have shown that over long timescales, optical variations lead the X-rays by 15 days for Mkn 509. Initially, this lag would appear to be far too large for reprocessing models where thermal optical/UV photons from the disk are inverse Compton scattered to X-ray energies (Haardt & Maraschi 1991).

However, such a lag is not unprecedented. Shemmer et al. (2003) found an optical to X-ray lag of 2.1 days in NGC 4051. Such a lag is most likely related to the viscous or thermal timescale. In that case, as variations in the accretion flow propagate inwards through the disk, they pass first through the optical emitting region, and then later through the X-ray

emitting region closer to the black hole. The additional high-frequency variability seen in the X-rays could come from the decreased light-travel time closer to the black hole, or from an additional emission component closer to the central engine.

If the lag is due to changes in the accretion flow, wouldn't we expect to find such a lag in all Seyfert galaxies? Probably not, since the mass of the black hole in Mkn 509 is $1.43 \times 10^8 M_{\odot}$ (Peterson et al. 2004), roughly an order of magnitude greater than previously studied objects. Many of the relevant timescales (orbital, thermal, viscous) increase linearly with mass, so we would expect to see lags of 1-2 days for other, less massive Seyferts.

Previous observing campaigns have involved weekly monitoring for a period of years, or more intensive monitoring for a period of a few days. In those cases, it is distinctly possible that the data would appear to be correlated, but with zero lag if the monitoring is on a weekly basis. Conversely, the data would appear to be uncorrelated if the lag time is greater than the monitoring period of just a few days. By observing a more massive galaxy on a frequent basis for several years, we have been able to measure a lag between the optical and X-ray emission.

We thank the referee for a useful report, which improved the readability of this paper. KM, WRT, and HRM acknowledge support from NASA grant No. NNG-04-G04-6G, and from the PEGA program at GSU.

REFERENCES

- Arévalo, P., Papadakis, I., Kuhlbrodt, B., & Brinkmann, W. 2005, *A&A*, 430, 435
- Chiang, J., Reynolds, C. S., Blaes, O. M., Nowak, M. A., Murray, N., Madejski, G., Marshall, H. L., & Magdziarz, P. 2000, *ApJ*, 528, 292
- Cooke, B. A., Ricketts, M. J., Maccacaro, T., Pye, J. P., Elvis, M., Watson, M. G., Griffiths, R. E., Pounds, K. A., McHardy, I., Maccagni, D., Seward, F. D., Page, C. G., & Turner, M. J. L. 1978, *MNRAS*, 182, 489
- Edelson, R. A., & Krolik, J. H. 1988, *ApJ*, 333, 646
- Haardt, F., & Maraschi, L. 1991, *ApJ*, 380, L51
- . 1993, *ApJ*, 413, 507
- Malkan, M. A. 1983, *ApJ*, 268, 582

- Maoz, D., Markowitz, A., Edelson, R., & Nandra, K. 2002, *AJ*, 124, 1988
- Markowitz, A., & Edelson, R. 2004, *ApJ*, 617, 939
- Markowitz, A., Edelson, R., Vaughan, S., Uttley, P., George, I. M., Griffiths, R. E., Kaspi, S., Lawrence, A., McHardy, I., Nandra, K., Pounds, K., Reeves, J., Schurch, N., & Warwick, R. 2003, *ApJ*, 593, 96
- Miller, H. R. 1981, *AJ*, 86, 87
- Papadakis, I. E., Brinkmann, W., Negoro, H., Detsis, E., Papamastorakis, I., & Gliozzi, M. 2000, *ArXiv Astrophysics e-prints*
- Peterson, B. M., Ferrarese, L., Gilbert, K. M., Kaspi, S., Malkan, M. A., Maoz, D., Merritt, D., Netzer, H., Onken, C. A., Pogge, R. W., Vestergaard, M., & Wandel, A. 2004, *ApJ*, 613, 682
- Peterson, B. M., McHardy, I. M., Wilkes, B. J., Berlind, P., Bertram, R., Calkins, M., Collier, S. J., Huchra, J. P., Mathur, S., Papadakis, I., Peters, J., Pogge, R. W., Romano, P., Tokarz, S., Uttley, P., Vestergaard, M., & Wagner, R. M. 2000, *ApJ*, 542, 161
- Pounds, K., Reeves, J., O'Brien, P., Page, K., Turner, M., & Nayakshin, S. 2001, *ApJ*, 559, 181
- Pounds, K. A., Nandra, K., Fink, H. H., & Makino, F. 1994, *MNRAS*, 267, 193
- Reynolds, C. S. 1997, *MNRAS*, 286, 513
- Shemmer, O., Uttley, P., Netzer, H., & McHardy, I. M. 2003, *MNRAS*, 343, 1341
- Shields, G. A. 1978, *Nature*, 272, 706
- Singh, K. P., Westergaard, N. J., Schnopper, H. W., Awaki, H., & Tawara, Y. 1989, in *ESA Special Publication*, Vol. 296, *ESA Special Publication*, ed. J. Hunt & B. Battrock, 1053–1058
- Timmer, J., & Koenig, M. 1995, *A&A*, 300, 707
- Uttley, P., Edelson, R., McHardy, I. M., Peterson, B. M., & Markowitz, A. 2003, *ApJ*, 584, L53
- Uttley, P., & McHardy, I. M. 2005, *MNRAS*, 363, 586

Uttley, P., McHardy, I. M., & Papadakis, I. E. 2002, MNRAS, 332, 231

Table 1. Optical Data

MJD ^a	obj-chkA ^b	obj-chkF ^b	chkA-chkF ^b
52939.57464	-1.152	-3.165	-2.013
52942.55968	-1.161	-3.184	-2.024
52945.53301	-1.185	-3.197	-2.012
52948.54159	-1.202	-3.211	-2.009
52951.53280	-1.212	-3.233	-2.021
52954.52887	-1.221	-3.231	-2.011
52957.52418	-1.241	-3.243	-2.002
52961.51394	-1.244	-3.264	-2.020
52964.50961	-1.240	-3.322	-2.082
52968.51123	-1.256	-3.235	-1.979
52972.51042	-1.257	-3.158	-1.901
52975.51269	-1.270	-3.319	-2.049
52978.51179	-1.226	-3.478	-2.253
52982.50990	-1.208	-3.783	-2.575
53125.85882	-1.142	-3.157	-2.015
53130.87646	-1.150	-3.158	-2.008
53134.79642	-1.148	-3.149	-2.001
53142.88867	-1.132	-3.135	-2.003
53153.90404	-1.092	-3.101	-2.009
53157.88565	-1.117	-3.111	-1.994
53160.81833	-1.113	-3.117	-2.004
53174.87961	-1.107	-3.128	-2.021
53180.83470	-1.111	-3.120	-2.009
53188.82977	-1.112	-3.135	-2.023
53191.82883	-1.104	-3.129	-2.025
53194.81454	-1.123	-3.147	-2.024
53197.85733	-1.150	-3.160	-2.010
53206.83395	-1.182	-3.178	-1.996
53217.76241	-1.194	-3.139	-1.945
53223.79976	-1.193	-3.210	-2.018
53240.77539	-1.193	-3.199	-2.006
53243.72964	-1.193	-3.222	-2.029
53246.72076	-1.151	-3.300	-2.149
53248.71606	-1.182	-3.207	-2.024
53250.70876	-1.182	-3.192	-2.010
53254.71429	-1.164	-3.177	-2.013
53262.69859	-1.153	-3.160	-2.006
53265.71466	-1.139	-3.110	-1.971
53268.68162	-1.149	-3.171	-2.022
53269.73045	-1.133	-3.156	-2.023
53274.68698	-1.143	-3.208	-2.064
53278.63685	-1.137	-3.152	-2.015
53281.65461	-1.158	-3.169	-2.012
53289.59618	-1.143	-3.152	-2.009
53296.60557	-1.139	-3.151	-2.012
53298.59711	-1.145	-3.151	-2.006

Table 1—Continued

MJD ^a	obj-chkA ^b	obj-chkF ^b	chkA-chkF ^b
53301.60686	-1.170	-3.176	-2.006
53307.60839	-1.174	-3.174	-2.000
53311.58837	-1.173	-3.185	-2.012
53324.53841	-1.151	-3.148	-1.997
53329.52019	-1.153	-3.176	-2.023
53560.85358	-0.974	-2.993	-2.019
53563.85279	-0.949	-2.959	-2.010
53570.74097	-0.912	-2.900	-1.988
53575.76890	-0.868	-2.879	-2.011
53578.82825	-0.842	-2.844	-2.002
53581.71973	-0.831	-2.858	-2.028
53584.72747	-0.819	-2.838	-2.019
53587.76697	-0.828	-2.849	-2.021
53588.73949	-0.842	-2.819	-1.977
53591.69279	-0.847	-2.836	-1.990
53599.76873	-0.821	-2.805	-1.984
53608.74477	-0.814	-2.812	-1.998
53618.72031	-0.824	-2.823	-1.999
53626.66931	-0.832	-2.851	-2.019
53633.60940	-0.861	-2.853	-1.992
53640.60154	-0.890	-2.826	-1.936
53644.59138	-0.920	-2.906	-1.986
53654.56947	-0.916	-2.924	-2.008
53661.58605	-0.916	-2.919	-2.002
53668.53228	-0.945	-2.945	-2.000
53676.52679	-0.917	-2.922	-2.005
53682.53441	-0.888	-2.923	-2.035
53704.52323	-0.850	-2.870	-2.020
53946.76870	-0.988	-2.979	-1.991
53951.66911	-0.962	-2.963	-2.001
53960.75079	-0.982	-2.988	-2.006
53963.71572	-0.978	-2.961	-1.983
53968.71505	-0.947	-2.951	-2.004
53970.75606	-0.932	-2.943	-2.011
53974.72391	-0.922	-2.933	-2.011
53979.69105	-0.918	-2.929	-2.012
53986.64399	-0.947	-2.854	-1.907
53989.68397	-0.949	-2.987	-2.038
53993.66439	-0.982	-2.986	-2.004
53998.61144	-1.004	-3.005	-2.001
54003.62051	-1.035	-3.028	-1.993
54007.64488	-1.051	-3.037	-1.985
54016.57288	-1.085	-3.086	-2.002
54019.57759	-1.082	-3.087	-2.005
54023.54125	-1.069	-3.081	-2.012
54026.54558	-1.079	-3.090	-2.010

Table 1—Continued

MJD ^a	obj-chkA ^b	obj-chkF ^b	chkA-chkF ^b
54029.51316	-1.077	-3.079	-2.001
54032.54927	-1.030	-3.051	-2.021
54037.50093	-1.061	-3.082	-2.022
54040.51623	-1.075	-3.027	-1.952
54043.50410	-1.075	-3.077	-2.002
54046.51196	-1.076	-3.089	-2.013
54051.50853	-1.075	-3.096	-2.021

^aModified Julian Date

^bErrors for photometry are given by the standard deviation of $\text{chkA} - \text{chkF}$ which is 0.026 mag.

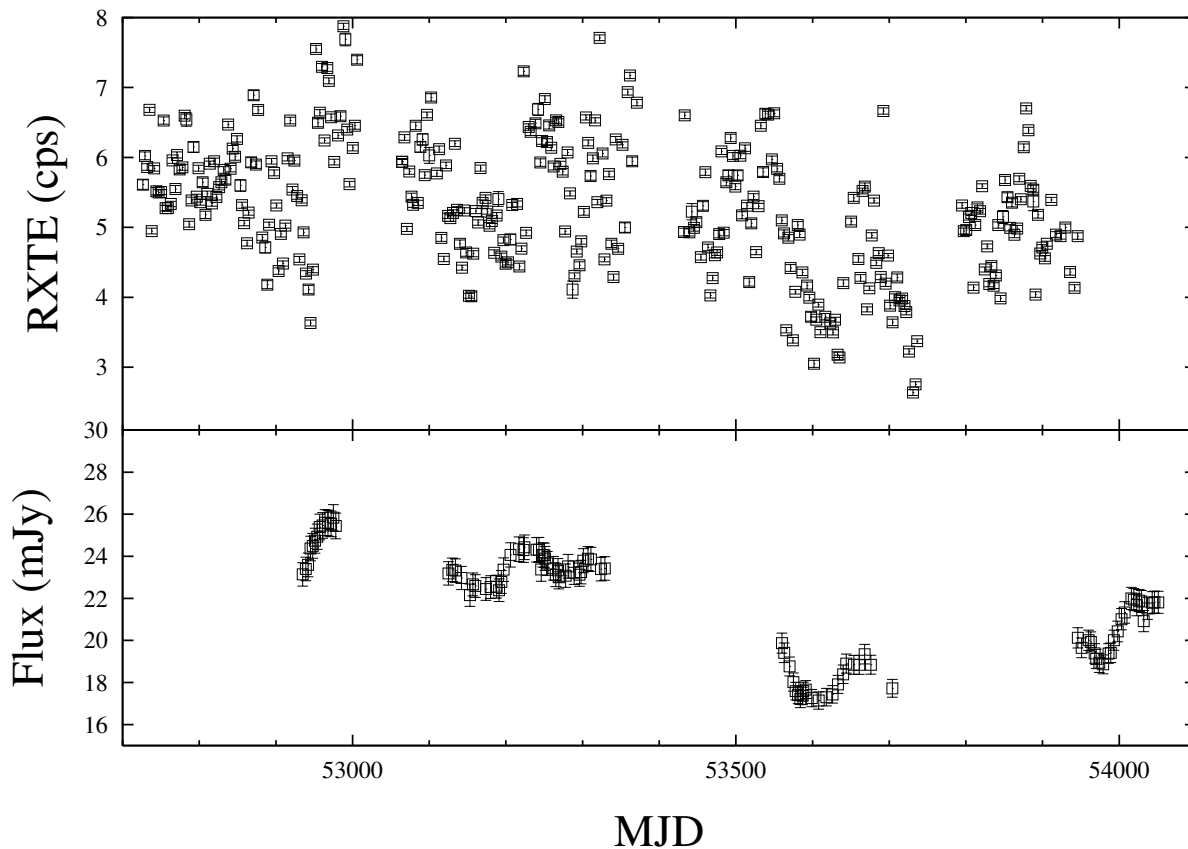


Fig. 1.— X-ray (top) and R-band optical (bottom) light curves for Mkn 509. Units are counts/sec/PCU and milli-Janskys for X-ray and optical data, respectively.

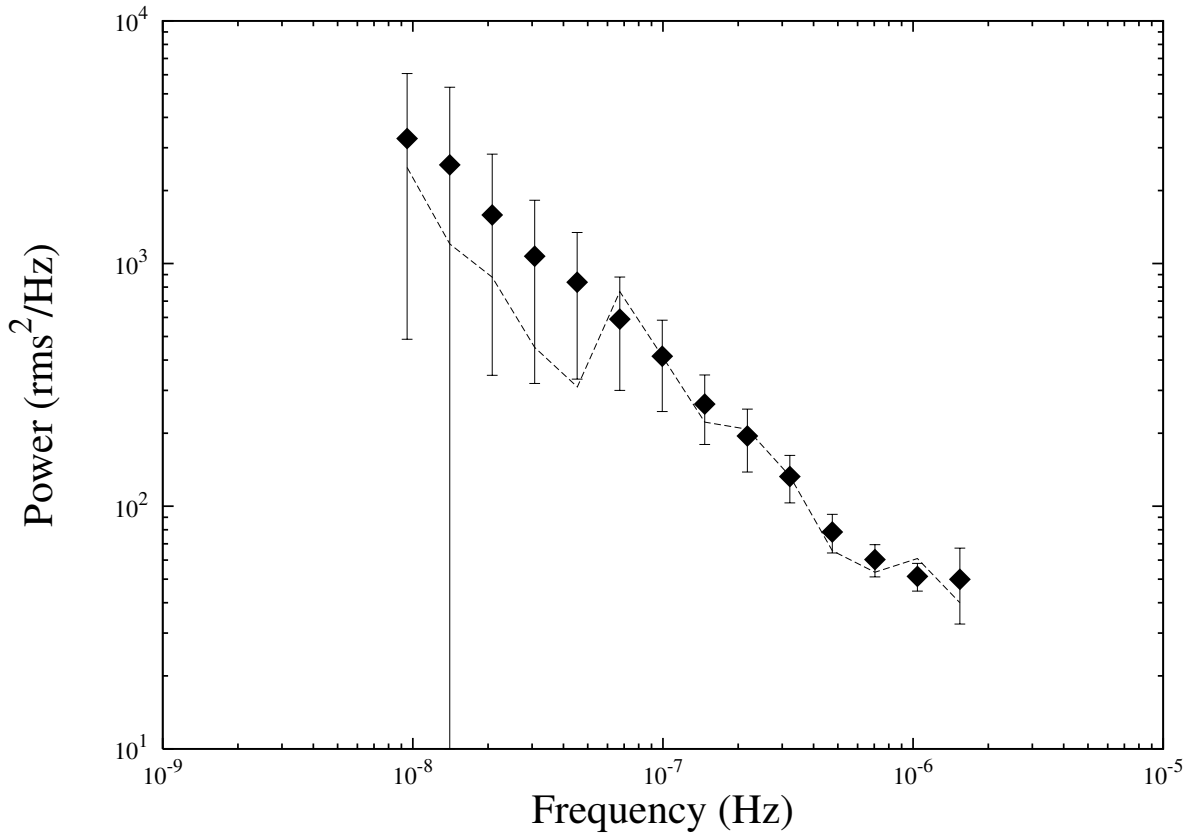


Fig. 2.— X-ray power density spectrum. Dashed line represents observed PDS, while points with error bars represent simulation results. Best fit model has a high-frequency slope of -2.0 , with a break frequency of $\log \nu_b = -6.47$.

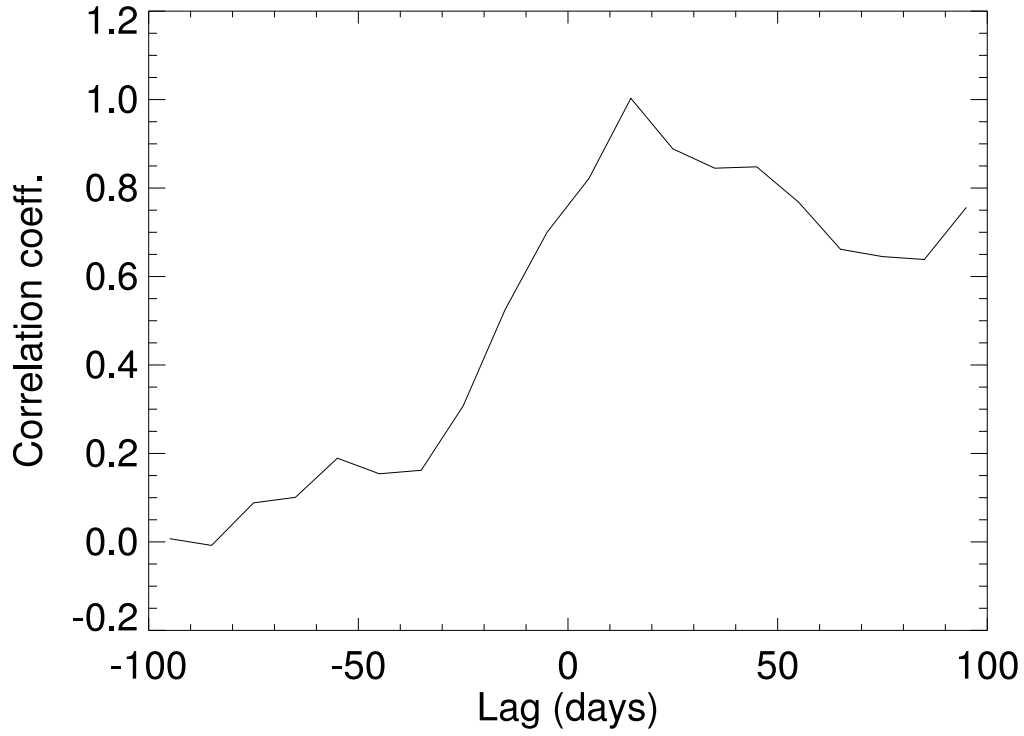


Fig. 3.— Discrete correlation function for X-ray and optical light curves. Positive lag indicates optical leading X-ray variations. See text for a discussion of errors.